7,7'-Bis[(aza-18-crown-6)carbonyl]thioindigo: Synthesis, Experimental, Theoretical Characterization and Biological Activities

Metin Koparır

Firat University, Faculty of Science, Department of Chemistry, 23169, Elazig, Turkiye

Abstract

*This work presents the characterization of 7,7'-Bis[(aza-18-crown-6)carbonyl]thioindigo (**I**) by quantum chemical calculations and spectral techniques. The molecular geometry, frontier molecular orbitals (FMO), molecular electrostatic potentials (MEP) and nonlinear optical properties of **I** in the ground state have been calculated using the density functional method (B3LYP) with the 6−31G(d,p) basis set. The calculated results show that the optimized geometry can well reproduce the crystal structure. The predicted non-linear optical properties of **I** are greater than ones of urea. The title compound has been tested in vitro for biological effects. The title compound was found to exhibit significant antimicrobial and antioxidant activity*

Keywords: 7,7'-bis[(aza-18-crown-6)carbonyl]thioindigo, dft, biological effects, mep

Corresponding Address: Metin Koparır, Firat University, Faculty of Science, Department of Chemistry, 23169, Elazig, Turkey
E-mail:mkoparir@hotmail.com

Introduction

The crown ether family is an appealing class of structures owing to their inherent and practical properties. As series of unusual ligand, they were the first synthetic structures contributing to the vastly increasing field of host-guest and molecular recognition chemistry [1-4]. Among the earliest-recognized remarkable properties of these molecules is their ability to selectively bind metal cations in solution. The applications in other fields, such as the synthetic, analytical, and physical organic chemistry [5-7] also cannot be ignored. For their pre-organized structures, crown ether is currently a popular molecular platform for designing novel receptors [8]. Molecular recognition is now verified by highly diversified and tailor-made structural component [9], but due to their generally good solubility requirement in many solvents, simple crown compounds are still attractive.

In recent years, density functional theory (DFT) has been extensively used in theoretical modeling. The development of better exchange–correlation functionals has made it possible to calculate many molecular properties with comparable accuracies to traditionally correlated *ab initio* methods, with more favorable computational costs [10]. Literature survey has revealed that the DFT has a great accuracy in reproducing the experimental values in geometry, dipole moment, vibrational frequency, etc. [11-15].

The aim of this study is to investigate the energetic and structural properties of the crown compound, 7,7'-bis[(aza-18-crown-6)carbonyl]thioindigo (Fig 1), using density functional theory calculations. In this study, the optimized geometry, frontier molecular orbitals (FMO), molecular electrostatic potentials (MEP) and nonlinear optical properties of **I** have been studied. These calculations are valuable for providing insight into molecular properties of crown ether compounds.

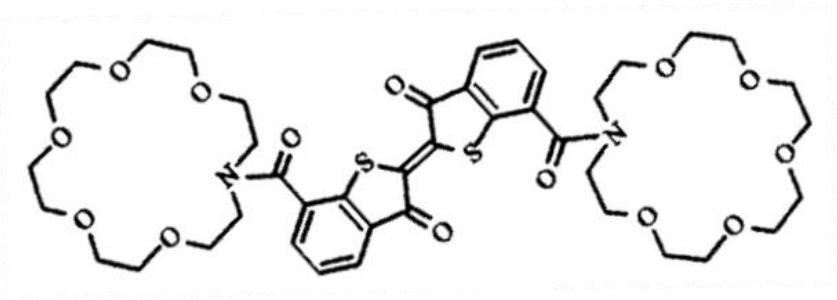

Figure 1. Chemical diagram of 7,7'-bis[(aza-18-crown-6)carbonyl]thioindigo.

Materials And Methods

Physical Measurements and Synthesis

Melting points were determined on a Thomas Hoover melting point apparatus and uncorrected, but checked by differential scanning calorimeter (DSC). The I.R. spectra were measured with Perkin–Elmer Spectrum one FT–IR spectrophotometer. Electronic spectral studies were conducted on a Shimadzu model UV-1700 spectrophotometer in the wavelength 1100–200 nm. The ^{1}H and ^{13}C spectra were taken on Bruker AC-400 NMR spectrometer operating at 400 MHz for ^{1}H, 100 MHz for ^{13}C NMR. Compound was dissolved in $CDCl_3$ and chemical shifts were referenced to TMS (^{1}H and ^{13}C NMR). Starting chemicals were obtained from Merck or Aldrich. 7,7'-bis[(aza-18-crown-6)carbonyl]thioindigo (**I**) was prepared according to a method given in the literature [16].

1-Aza-18-crown-6 was acylated with 7,7'-bis(chlorocarbonyl)-thioindigo in refluxing pyridine. The residue was purified via column chromatography on (SiO_2, 6:1 ethyl acetate:ethanol) afforded the title compound. Crystals were obtained by slow evaporation of a dilute benzene solution. Yield 46%, m.p. 405-407 K; ^{1}H NMR (400 MHz, $CDCI_3$/TMS): δ (ppm.) 7.94 (2H, d, J = 7.5 Hz), 7.67 (2H, d, J = 7.5 Hz), 7.40 (2H, t, J = 7.5 Hz), 3.73 (*bs*,48H); ^{13}CNMR (100 MHz, $CDCI_3$/TMS): δ (ppm) 189.3, 168.1, 146.3, 133.9, 133.1, 132.8, 128.9, 126.9, 126.1, 70.6, 49.9, 45.9; IR (KBr): 1663, 1628, 1271, 1109 cm^{-1}.

Computational methods

The molecular geometry was taken directly from the X-ray diffraction experimental result without any constraints. In the next step, the DFT calculations with a hybrid functional B3LYP (Becke's Three parameter hybrid functional using the LYP correlation functional) with the 6–31G(d,p) basis set using the Berny method [17,18] were performed with the Gaussian 09W software package [19]. To investigate the reactive sites of **I** the molecular electrostatic potentials were evaluated using B3LYP/6–31G(d,p) method. The mean linear polarizability and mean first hyperpolarizability properties of **I** were obtained from molecular polarizabilities based on theoretical calculations. In addition, frontier molecular orbitals (FMO) for the title compound were performed with B3LYP/6-31G(d,p) the optimized structure.

In vitro antimicrobial activity

Isolated bacteria used in this study were obtained from the forensic medicine institute in Malatya. The clinical isolates (*Shigella dysenteriae, Escherichia coli, Proteus vulgaris, Serratia* spp., *Klebsiella, Pseudomonas aeruguinosa, Staphylococcus aureus*) were grown in Mueller–Hinton Broth media for 24h at 37°C. Antimicrobial activities of the title compound was estimated by a Minimum Inhibitory Concentration (MIC, μg/mL) using a micro-broth dilution method and essentially following the guidelines of Hannan [20]. A stock solution of each antimicrobial in DMSO was prepared according to NCCLS guidelines [21]. The MIC was carried out in standard sterile 96 well flat bottom microtitre plates and the layout was designed so that each row covered the final antimicrobial dilution of 500–0.5 μg/mL with one control well. Using sterilized micropipette, a 40 μL of the selected antimicrobial with the correct concentration was added to each well and another well was loaded with the same volume of control (DMSO solvent). Then a 150 μL of Mueller Hinton media was added to all wells, followed by a 10 μL (10^8 cfu/mL) of the bacterial culture giving a final concentration of 5×10^7 cfu/mL of bacteria in the well. The plates were sealed and incubated at 37 °C under atmospheric conditions. After 24h incubation the microtitre plates were read using the eliza reader. The minimal concentration that has optical density less than that of the control was defined as the MIC.

DPPH free radical scavenging activity

Free radical scavenging activity of the title compound was determined by measuring the change in the absorbance of DPPH$^{\bullet}$ (1,1-diphenyl-2-picrylhydrazylradical) at 517 nm spectrophotometrically. Stock solutions of 500 μM of tested sample and DPPH$^{\bullet}$ were prepared in DMSO. 400 μL of DPPH$^{\bullet}$ solution was added to sample solution at different concentrations (500, 1000, 1500, 2000 and 2500 μL) and appropriately diluted with DMSO to total volume of 4.0 mL. A 400 μL from DPPH$^{\bullet}$ stock solution was also diluted to 4.0 mL using DMSO solvent to make the control. The reaction mixtures were thoroughly mixed by shaking the test tubes vigorously and incubated at 25 °C for 60 min in a water bath in the dark. Absorbance at 517 nm was measured and the solvent was corrected throughout. The scavenging effect was calculated using the following equation [22]:

$$Scavenging\ activity\ (\%) = \frac{A_0 - A_s}{A_0} \times 100¶$$

where A_s is the absorbance of the $DPPH^{\bullet}$ in the presence of the tested compound and A_0 is the absorbance of the $DPPH^{\bullet}$ in the absence of the tested compound (control). The data for antioxidation presented as means ± SD of three determinations

Results

Description of the crystal structure

The crystal structure of **I** is triclinic and space group P1, M_w = 875,03, a = 9.267 (2) Å, b = 10.344 (3) Å, c = 12.149 (2) Å, β= 104.51 (2), and V= 1062.7(5) $Å^3$, Dx = 1.367 g/cm^{-3}. Additional information for the structure determinations are given in Table 1. The title compound is centrosymmetric and possesses inversion symmetry (Fig 2A). The thioindigo skeleton is essentially planar, deviations from the best least-squares plane being <0.07 Å. These results are in agreement with the X-ray structures of thioindigo [23] and 7,7'-dimethylthioindigo [24]. Steric effects force the 7,7'-bis(aza-18-crown-6)carbonyl groups from planarity [C(8)–C(7)–C(9)–O(2) and C(6)–C(7)–C(9)–O(2) torsion angles of -45.0 (5) and 127.8 (4)°, respectively]. The aza-crown ether portion exhibited disorder at three positions, making structural details less certain [C(15)–C(15)' 0.71 (2), C(18)–C(18)' 1.05(2), O(5)–O(5)' 1.22 (1)Å.]. Comparisons with reported crystallographic studies on aza-crown derivatives revealed similar properties [25].

Table 1. Crystallographic data for title compound [16].

Chemical formula	$C_{42}H_{54}N_2O_{14}S_2$
Formula weight	875.03
Temperature (K)	293
Crystal system	Triclinic
Space group	P1
Unit cell parameters	
a (Å)	9.267 (2)
b (Å)	10.344 (3)
c (Å)	12.149 (2)
β(°)	104.51 (2)
Volume ($Å^3$)	1062.7 (5)
Z	1
Dcalc (g/cm^3)	1.367
Crystal size (mm)	0.38 ×0.17 × 0.07
Reflections observed [I >3σ(I)]	2955
Data/parameters	1994/298
R [F^2>2σ(F^2)]	0.015
wR (F^2)	0.067
Goodness-of-fit on Indicator	0.03
Structure determination	SHELX97
Refinement	Full matrix
Δ*p* max, Δ*p* min (e/ $Å^3$)	0.37, -0.24

Optimized Geometry

The optimized parameters (bond lengths and bond angles) of **I** were obtained using the B3LYP/6−31G(d,p) method. The atomic numbering scheme of the theoretical geometric structure is shown in Fig 2B. Calculated geometric parameters are listed in Table 2 along with the experimental data. When the X-ray structure of **I** is compared with its optimized counterparts (see Fig 3), slight conformational discrepancies are observed between them. We note that the experimental results are for the solid phase and the theoretical calculations are for the gas phase. In the solid state, the existence of a crystal field along with the intermolecular interactions connects the molecules together, which results in the differences in bond parameters between the calculated and experimental values.

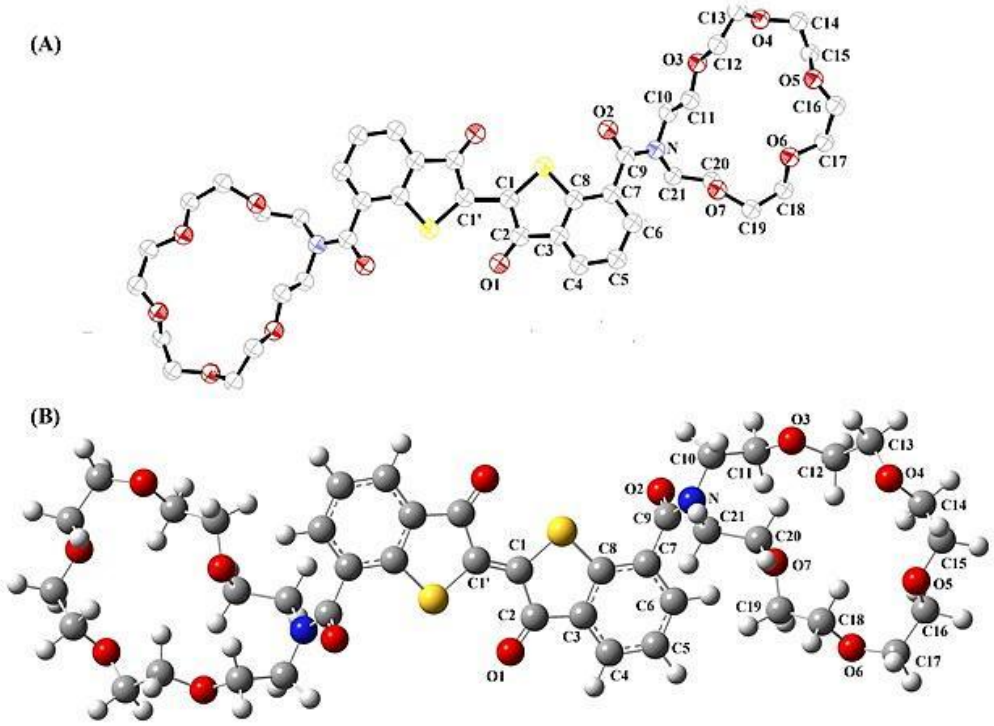

Figure 2. (A) Ortep-3 diagram of the title compound (B) The theoretical -geometric structure of the title compound (with B3LYP/6–31G(d,p) level).

A logical method for globally comparing the structures obtained with the theoretical calculations is by superimposing the molecular skeleton with that obtained from X-ray diffraction, giving a RMSE of 0.355 Å for B3LYP/6−31G(d,p) (Fig 3). This magnitude of RMSE can be explained by the fact that the intermolecular Coulombic interaction with the

Table 2. Selected molecular structure parameters.

Parameters	Experimental	B3LYP/6-31G(d,p)
Bond lengths (Å)		
C(1)-C(1')	1.350 (5)	1.329
C(1)-C(2)	1.489 (5)	1.502
C(1)-S	1.744 (4)	1.770
C(2)-O(1)	1.221 (4)	1.206
C(2)-C(3)	1.466 (5)	1.485
C(3)-C(4)	1.373 (6)	1.394
C(3)-C(8)	1.397 (5)	1.409
C(4)-C(5)	1.379 (6)	1.403
C(5)-C(6)	1.399 (6)	1.397
C(6)-C(7)	1.384 (6)	1.409
C(7)-C(8)	1.404 (5)	1.386
C(7)-C(9)	1.502 (5)	1.498
C(8)-S	1.764 (4)	1.770
C(9)-O(2)	1.223 (59	1.221
C(9)-N	1.348 (4)	1.402
N-C(10)	1.454 (5)	1.481
N-C(21)	1.473 (5)	1.486
RMSE[a]		0.013
Bond Angles (°)		
C(1')-C(1)-C(2)	123.3 (3)	130.2
C(1')-C(1)-S	124.3 (3)	117.6
C(2)-C(1)-S	112.4 (3)	112.2
C(1)-C(2)-O(1)	123.2 (4)	124.1
C(1)-C(2)-C(3)	110.1 (3)	108.7
O(1)-C(2)-C(3)	126.7 (4)	127.2
C(6)-C(7)-C(9)	124.0 (4)	119.9
C(8)-C(7)-C(9)	117.5 (3)	121.6
C(3)-C(8)-C(7)	119.9 (4)	121.2
C(3)-C(8)-S	114.7 (3)	112.8
C(7)-C(8)-S	125.5 (3)	125.9
C(1)-S-C(8)	91.0 (2)	92.1
C(2)-C(3)-C(4)	127.2 (3)	125.6
C(2)-C(3)-C(8)	111.9 (3)	114.2
C(4)-C(3)-C(8)	120.9 (3)	120.2
C(3)-C(4)-C(5)	119.9 (4)	118.9
C(4)-C(5)-C(6)	119.6 (4)	120.6
C(5)-C(6)-C(7)	121.4 (4)	120.6
C(6)-C(7)-C(8)	118.2 (3)	118.5
C(7)-C(9)-O(2)	118.4 (3)	122.6
C(7)-C(9)-N	120.6 (3)	117.5
O(2)-C(9)-N	121.0 (4)	119.8
C(9)-N-C(10)	125.1 (3)	123.4
C(9)-N-C(21)	116.9 (3)	117.6
C(10)-N-C(21)	117.7 (3)	117.6

[a] Between the bond lengths and the bond angles computed by the theoretical method and those obtained from X-ray diffraction.

neighboring molecules are absent in gas phase, whereas the experimental result corresponds to interacting molecules in the crystal lattice [26].

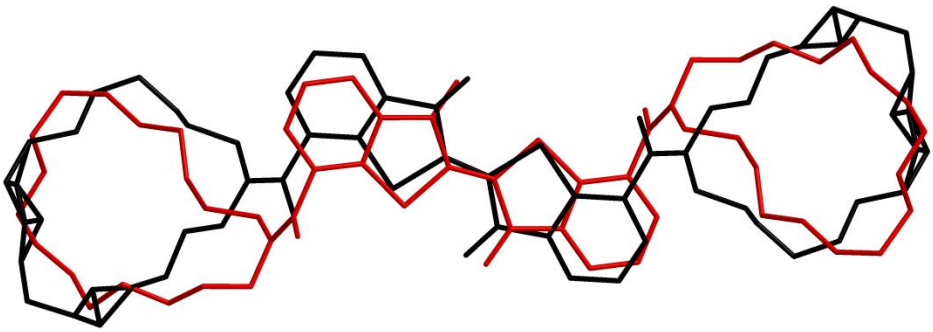

Figure 3. Atom-by-atom superimposition of the structures calculated (red) over the X-ray structure (black) for the title compound. Hydrogen atoms omitted for clarity

Molecular electrostatic potential

Molecular electrostatic used extensively for interpreting potentials have been and predicting the reactive behavior of a wide variety of chemical system in both electrophilic and nucleophilic reactions, the study of biological recognition processes and hydrogen bonding interactions [27].

V*(*r*)**, at a given point ***r*(*x,y,z*)** in the vicinity of a molecule, is defined in terms of the interaction energy between the electrical charge generated from the molecule electrons and nuclei and positive test charge (a proton) located at ***r. Unlike many of the other quantities used at present and earlier as indices of reactivity, ***V*(*r*)** is a real physical property that can be determined experimentally by diffraction or by computational methods. For the systems studied the MEP values were calculated as described previously, using the equation [28]:

$$V(r) = \sum \frac{Z_A}{|R_A - r|} - \int \frac{\rho(r')}{|r' - r|} dr'$$

where the summation runs over all the nuclei ***A*** in the molecule and polarization and reorganization effects are neglected. Z_A is the charge of the nucleus ***A***, located at R_A and $\rho(r')$ is the electron density function of the molecule. To predict reactive sites for electrophilic and nucleophilic attack for the investigated molecule, molecular electrostatic potential (MEP) was calculated at B3LYP/6-31G(d,p) optimized geometries. Red and blue areas in the MEP map refer to the regions of negative and positive potentials and correspond to the electron-rich and

electron-poor regions, respectively, whereas the green color signifies the neutral electrostatic potential. The MEP surface provides necessary information about the reactive sites.

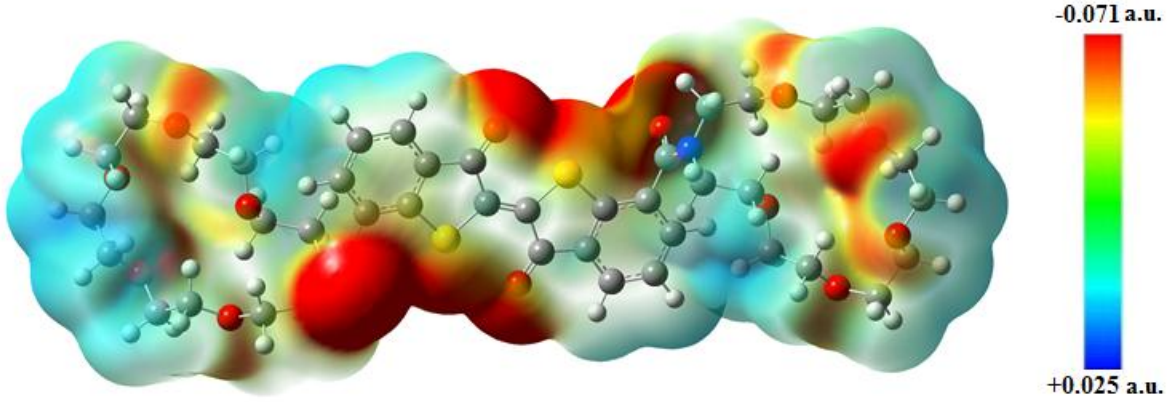

Figure 4. Molecular electrostatic potential map calculated at B3LYP/6-31G(d,p) level.

The negative regions ***V(r)*** were related to electrophilic reactivity and the positive ones to nucleophilic reactivity. As easily can be seen in Fig 4, this molecule has several possible sites for electrophilic attack in which ***V(r)*** calculations have provided in-sights. Negative regions in the studied molecule were found around the carbonyl group and S atom. The negative ***V(r)*** values are −0.071 a.u. for carbonyl groups, which is the most negative region, −0.040 a.u. for S atom which is a less negative region. However, a maximum positive region is localized on the H atom of the ether group with a value of +0.025 a.u. indicating a possible site for nucleophilic attack. According to these calculated results, the MEP map shows that the negative potential sites are on electronegative atoms as well as the positive potential sites are around the hydrogen atoms. These sites give information about the region from where the compound can have intermolecular interactions.

Frontier molecular orbitals

In principle, there are several ways to calculate the excitation energies. The simplest one involves the difference between the highest occupied molecular orbital (HOMO) and the lowest unoccupied molecular orbital (LUMO) of a neutral system, which is a key parameter in determining molecular properties [29]. Moreover, the Eigen values of HOMO (π donor) and LUMO (π acceptor) and their energy gap reflect the chemical activity of the molecules. Recently, the energy gap between HOMO and LUMO has been used to prove the bioactivity

from intra-molecular charge transfer (ICT) [30,31]. Fig 5 shows the distributions and energy levels of the HOMO–1, HOMO, LUMO and LUMO+1 orbitals computed at the B3LYP/6−31G(d,p) level for **I**. As seen from Fig 5, both in the HOMO and HOMO−1, electrons are delocalized on the thioindigo rings. For the LUMO and LUMO+1 electrons are mainly delocalized on the O1, C2, C1 and S atoms. The value of the energy separation between the HOMO and LUMO is 7.9177 eV. This large HOMO–LUMO gap automatically means high excitation energies for many of excited states, a good stability and a high chemical hardness for **I**.

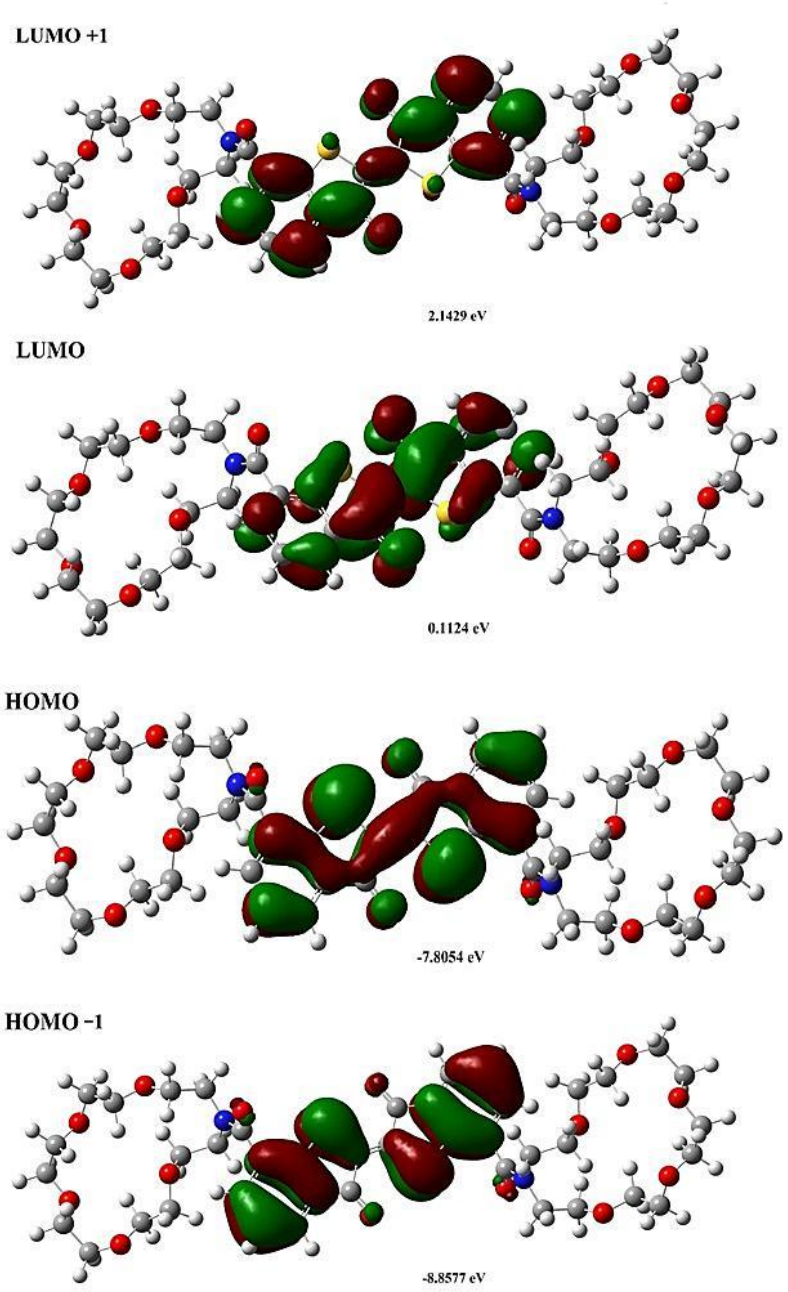

Figure 5. Molecular orbital surfaces and energy levels given for the HOMO, HOMO -1, LUMO and LUMO + 1 of the title compound computed at B3LYP/6-31G(d,p) level

Nonlinear optical effects)

NLO properties have been of great interest by the recent years. Because some synthesized novel materials show efficient nonlinear optical that are used telecommunication, potential applications in modern communication technology, optical signal processing and data storage.

The calculations of the total molecular dipole moment (μ), linear polarizability (α) and first-order hyperpolarizability (β) from the Gaussian output have been explained in detail previously [32], and DFT has been extensively used as an effective method to investigate the organic NLO materials. It is well known that from the literature, the B3LYP approach provides fairly reliable values in electric hyperpolarizability calculations when compared with accuracies of traditional *ab initio* methods and this predictive capability of widely used B3LYP method is of interest to a wide audience of computational scientists [33,34]. In addition, taking into account reliability and the computational time required [35], the basis set 6−31G(d,p) was chosen for the calculations of the hyperpolarizability in this study.

The electronic dipole moment μ_i(i = x, y, z), polarizability α_{ij} and the first hyperpolarizability β_{ijk} of **I** were calculated at the B3LYP/6−31G(d,p) level using Gaussian 09W program package. Urea is one of the prototypical molecules used in the study of the NLO properties of molecular systems. Therefore it was used frequently as a threshold value for comparative purposes. The calculated values of α_{tot} and β_{tot} for **I** are, 15.849 $Å^3$ and 1.850×10^{-30} cm^5/esu, which are greater than those of urea (the α_{tot} and β_{tot} of urea are 3.831 $Å^3$ and 0.37×10^{-30} cm^5/esu obtained by B3LYP/6−31G(d,p) method). According to the magnitude of the first hyperpolarizability, **I** may be a potential applicant in the development of NLO materials.

Biological study

Antimicrobial activity

The MIC of the title compound against different types of Gram-positive and Gram-negative bacteria were determined and tabulated in Table 3. The data indicate that the title compound showed moderate antimicrobial activity against *P. aereuguinosa* and *E.coli* bacteria, and showed no activity towards *P. vulgaris, S. dysen-teriae, S. aureus, Klebsiella* and *Serratia*.

Table 3
Minimum inhibitory concentration (MIC, µg/mL) data of the title compound against a number of bacteria.

(MIC, µg/mL)							
Tested Compound	Gram (-) bacteria						Gram (+) bacteria
	Sd	*Ps*	*Pv*	*E.coli*	*Serratia*	*Klebsiella*	*Sa*
Title Compound	N	62.5	N	62.5	N	62.5	N
Cephalexin	7.8	125	125	15.6	125	7.8	7.8
Cephradine	15.6	125	125	15.6	125	15.6	7.8

Sa - Staphylococcus aureus, Ps - Pseudomonas aeruguinosa, E. Coli - Escherichia coli, Sd - Shigella dysenteriae, Pv - Proteus vulgaris.
Cephalexin and Cephradine are standart antibiotics.
N. non detected

Antioxidant activity

Since the antioxidants are gaining a lot of importance as panacea for a large number of life-style diseases like aging, cancer, diabetes, cardiovascular and other degenerative diseases, it is of immense significance to establish some new antioxidants by a convenient synthetic methodology. Although a number of methods such as ORAC, ABTS, DMPD, FRAP, TRAP, TBA, superoxide radical scavenging, hydroxyl radical scavenging, nitric oxide radical scavenging, xanthine oxidase, cytochrome C, reducing power method, etc. available, the DPPH method is very common and proved as the best [36]. As shown in Table 4, the title compound has scavenging activity between 44.7% and 70.7% within the investigated concentration range. The antioxidant activity of the title compound is obvious that the scavenging activity increases with increasing sample concentration in the range tested**.**

Table 4
Antioxidant scavenging activity data of the title compound on $DPPH^{\bullet}$ free radical at different concentrations.

Tested Compound	DPPH scavenging activity (%)				
	62.5 µM	125 µM	187.5 µM	250 µM	312.5 µM
Title Compound	44.7 ± 0.4	51.1 ± 0.8	61.1 ± 0.4	66.9 ± 0.3	70.7 ± 0.5

Conclusions

In this study, the optimized geometry, frontier molecular orbitals (FMO), molecular electrostatic potentials (MEP) and nonlinear optical properties of **I** have been studied. Due to the lack of experimental information on the structural parameters available in the literature, the optimized geometric parameters (bond lengths and bond angles) was theoretically determined at B3LYP/6-31G(d,p) level of theory and compared with the structurally similar compounds. The X-ray structure is found to be slightly different from its optimized counterpart. It was noted here that the experimental results belong to solid phase and

theoretical calculations belong to gaseous phase. In the solid state, the existence of the crystal field along with the intermolecular interactions have connected the molecules together, which result in the differences of bond parameters between the calculated and experimental values. Despite the differences observed in the geometric parameters, the general agreement is good and the theoretical calculations support the solid-state structure. When all theoretical results scanned, they are showing good correlation with experimental data. The antimicrobial activity results show that title compound possessed moderate antibacterial activity. The antioxidant activity of the title compound is obvious that the scavenging activity increases with increasing sample concentration in the range tested.

References

1. Hong J, Song J, Ham S. Molecular recognition of ammonium ion by tetrahomodioxacalix[4]biscrown. Tetrahedron Lett. 2007; 48:1327-30.
2. Anderson JD, Paulsen ES, Dearden DV. Alkali metal binding energies of dibenzo-18-crown-6: experimental and computational results. Int. J. Mass Spectrom. 2003; 227:63-76.
3. Brodbelt J, Maleknia S. Gas-Phase selectivities of crown ethers for alkali-metal ion complexation. J. Am. Chem. Soc. 1192; 114:4295-8.
4. Takeda Y, Hashimoto K, Yoshiyama D, Katsuta S. Extraction of alkali metal (Li, Na, K) Picrates with benzo-15-crown-5 into various organic solvents. Elucidation of fundamental equilibria determining the extraction-ability and –selectivity. J. Incl. Phenom. Macro. 2002; 42:313-21.
5. Bourgoin M, Wong KH, HUI JY, SMID J. Interactions of macrobicyclic polyethers with ions and ion-pairs of picrate salts. J. Am. Chem. Soc. 1975; 97:3462-7.
6. Bandyopadhyay R, Cooper BFT, Rossini AJ, Schurko RW, Macdonald CLB. J. Organomet. Chem. 2010; 695:1012-8.
7. Dubonosov AD, Minkin VI, Bren VA, Shepelenko EN, Tsukanov AV, Starikov AG, Borodkin GS. Tautomeric crown-containing chemosensors for alkali-earth metal cations. Tetrahedron. 2008; 64:3160-7.
8. Sukwattanasinitt M, Rojanathanes R, Tuntulani T, Sritana-Anant Y, Ruangpornvisuti V. Synthesis of stilbene crown ether p-tert-butylcalix[4]arenes. Tetrahedron Lett. 2001; 42:5291-3.

9. Lehn JM. Perspectives in supramolecular chemistry – from molecular recognition towards molecular information-processing and self-organization. Angew. Chem. Int. Edit. 1990; 29:1304-19.
10. Proft FD, Geerlings P. Conceptual and computational DFT in the study of aromaticity. Chem. Rev. 2001; 101:1451-64.
11. Orek C, Koparir P, Koparir M. N-Cyclohexyl-2-[5-(4-pyridyl)-4-(p-tolyl)-4H-1,2,4-triazol-3-ylsulfanyl]-acetamide dihydrate:Synthesis, experimental, theoretical characterization and biological activities. Spectrochim Acta. A. 2012; 97:923-34.
12. Cansiz A, Cetin A, Orek C, Karatep M, Sarac K, Kus A, Koparir P. 6-Phenyl-3-(4-pyridyl)-1,2,4-triazolo-[3,4-b][1,3,4]thiadiazole: Synthesis, experimental, theoretical characterization and biological activities. Spectrochim Acta. A. 2012; 97:607-15.
13. Tanak H. DFT computational modeling studies on 4-(2,3-Dihydroxybenzylideneamino)-3-methyl-1H-1,2,4-triazol-5(4H)-one. Computational And Theoretical Chemistry. 2011; 967:93-101.
14. Andzelm J, Fitzgerald G. Chemical Applications of Density Funtional Theory - Comparison to Experiment, Hartree-Fock, and Perturbation-Theory. J. Phys. Chem. 1991; 95:10531-4.
15. Andzelm J, Wimmer E. Density Functional Gaussian-Type-Orbital Approach to Molecular Geometries, Vibrations, and Reaction Energies. J. Chem. Phys. 1992; 96:1280-303.
16. Bien JT, Shang MY, Smith BD. 7,7'-bis[(aza-18-crown-6)carbonyl]thio-indigo. Acta Crystallogr. C. 1996; 52(1):183-6.
17. Schlegel HB. Optimization of Equilibrium Geometries and Transition Structure. Journal of Computional Chemistry. 1996; 3:214-8.
18. Peng C, Ayala PY, Schlegel HB. Using Redundant Internal Coordinates to Optimize Equilibrium Geometries and Transition States. Journal of Computational Chemistry. 1996; 17:49-56.
19. Frisch MJ, Trucks GW, Schlegel HB, Scuseria GE, Robb MA, Cheeseman JR, Scalmani G, Barone V, Mennucci B, Petersson GA, Nakatsuji H, Caricato M, Li X, Hratchian HP, Izmaylov AF, Bloino J, Zheng G, Sonnenberg JL, Hada M, Ehara M, Toyata K, Fukuda R, Hasegawa J, Ishida M, Nakajima T, Honca Y, Kitao O, Nakai H, Vreven T, Montgomery JA, Peralta JE, Ogliaro F, Bearpark M, Heyd JJ, Brothers E, Kudin KN, Staroverov VN, Kobayashi R, Normand J, Raghavachari K, Rendell

A, Burant JC, Iyengar SS, Tomasi J, Cossi M, Rega N, Millam JM, Klene M, Knox JE, Cross JB, Bakken V, Adamo C, Jaramillo J, Gomperts R, Strarmann RE, Yazyev O, Austin AJ, Cammi R, Pomelli C, Ochterski JW, Martin RL, Morokuma K, Zakrzewski VG, Voth GA, Salvador P, Dannenberg JJ, Dapprich S, Daniels AD, Farkas O, Foresman JB, Ortiz JV, Cioslowski J and Fox DJ, Gaussian Inc, Wallingford CT.2009.

20. Woods GL, Washington JA, Antibacterial susceptibility tests: dilution and disk diffusion methods, in: Murray PR, Baron EJ, Pfaller MA, Tenover FC, Yolken RH, eds, 6th ed. American Society for Microbiology, Washington, 1995;1327-41.
21. Roberts J. The Cephalosporins in Kirk-Othmer Encyclopedia of Chemical Technology. 3nd ed. John Wiley & Sons Inc., 1992;28-82
22. M.M. Hossain, M.F. Aziz, R. Ahmed, M. Hossain, A. Mahmuda, T. Ahmed, M.H. Mazumder, Int. J. Pharm. Sci. 2 (2010) 60–3.
23. Haasewessel W, Ohmasa M, Süsse P. Thioindigo – crystal structural data for modification-2. Naturwissenschaften. 1977; 64:435
24. Süsse P, Neuling H. Crystal-structure of 7,7'-dimethylthioindigp. Z. Kristallogr. 1981; 154:308-10.
25. Gokel GW, Garcia BJ. Crown-cation complex effects .3. chemistry and complexes of monoaza-18-crown-6. Tetrahedron Lett. 1977; 77:317-28.
26. Tanak H. Crystal Structure, Spectroscopy, and Quantum Chemical Studies of €-2[(2-Chlorophenyl)iminomethyl]-4-trifluoromethoxyphenol. Journal of Physical Chemistrya. 2011; 115:13865-76.
27. Politzer P, Murray JS. Theoretical biochemistry and molecular biophysics: a comprehensive survey. Adenine Press, Schenectady, NY, 1991.
28. Politzer P, Murray JS. The Fundamental Nature and Role of the Electorstatic Potential in Atoms and Molecules. Theor. Chem. Acc. 2002; 108:34.
29. Amalanathan M, Rastogi VK, Joe IH, Palafox MA, Tomar R. Density functional theory calculations and vibrational spectral analysis of 3,5-(dinitrobenzoic acid). Spectrochim Acta A. 2009; 78:1437-44.
30. Padmaja L, Ravikumar C, Sajan D, Joe IH, Jayakumar VS, Pettit GR, Nielsen OF. Density Functional Study on the Structural Conformations and Intramolecular Charge transfer From the Vibrational Spectra of the Anticancer Drug Combretastatin. J. Raman. Spectrosc. 2009; 40:419-28.

31. Sagdinc S, Pir H. Spectroscopic and DFT studies of flurbiprofen as dimer and its Cu(II) and Hg(II) complexes. Spectrochim Acta A. 2009; 73:181-7.
32. Thanthiriwatte KS, de Silva KMN. Non-linear Optical Properties of Novel Fluorenyl Derivatives - ab Initio Quantum Chemical Calculations. J. Mol. Struc-Theochem. 2002; 617:169-75.
33. Maroulis G, Begue D, Pouchan C. Accurate Dipole Polarizabilities of Small Silicon Clusters From ab Initio and Density Functional Theory Calculations. Journall of Chemical Physics. 2003; 119:794-8.
34. Maroulis G. How Large is the Static Electric (hyper)Polarizability Anisotropy in HXeI. Journal of Chemical Physics. 2008; 129:044313-21.
35. Qin C, Si Y, Yang G, Su Z. Quantum Chemical Study of Structures, Electronic Spectrum, and Nonlinear Optical Properties of Polynuclear Lithium Compounds. Computational and Theoretical Chemistry. 2011; 966:14-9.
36. Bondet V, Brandwilliams W, Berset C. Kinetics and mechanisms of antioxidant activity using the DPPH free radical method. Food Science and Technology-Lebensmittel-Wissenschaft & Technologie. 1997; 30:609-15.